Journal of
Synchrotron
Radiation

ISSN 0909-0495

Received 14 February 2005
Accepted 5 April 2005

Improving the performance of high-resolution X-ray spectrometers with position-sensitive pixel detectors

S. Huotari,* Gy. Vankó, F. Albergamo, C. Ponchut, H. Graafsma, C. Henriquet, R. Verbeni and G. Monaco

European Synchrotron Radiation Facility, BP 220, F-38043 Grenoble CEDEX 9, France.
E-mail: huotari@esrf.fr

A dispersion-compensation method to remove the cube-size effect from the resolution function of diced analyzer crystals using a position-sensitive two-dimensional pixel detector is presented. For demonstration, a resolution of 23 meV was achieved with a spectrometer based on a 1 m Rowland circle and a diced Si(555) analyzer crystal in a near-backscattering geometry, with a Bragg angle of 88.5°. In this geometry the spectrometer equipped with a traditional position-insensitive detector provides a resolution of 190 meV. The dispersion-compensation method thus allows a substantial increase in the resolving power without any loss of signal intensity.

Keywords: X-ray spectrometers; diced analyzer crystals; position-sensitive detectors.

1. Introduction

Most high-resolution X-ray spectrometers today are based on crystal analyzers operating in the Rowland circle geometry, which allows for a simultaneous focusing and energy analysis of X-rays coming from a point source. A practical method of choice to realise the Rowland geometry is the Johann approximation (Johann, 1931), where an analyzer crystal is spherically or cylindrically bent with a bending radius R equal to the Rowland circle diameter. Assuming the analyzer crystal size to be much smaller than its bending radius, to a good approximation all X-rays reflected by the analyzer crystal have the same Bragg angle and are focused at the same point, which also lies on the Rowland circle. However, bending a crystal always results in elastic deformations that affect the energy resolution, leading to a relatively large bandwidth being reflected (Suortti & Freund, 1989),

$$\Delta E/E = (l/R)\left|\cot^2\theta_{\rm B} - \nu\right|, \qquad (1)$$

where l is the effective thickness of the crystal, $\theta_{\rm B}$ is the Bragg angle and ν is the Poisson ratio of the analyzer crystal material. In order to circumvent this distortion error and obtain the highest possible resolution in the Rowland circle geometry, the method of choice seems to be to use so-called diced analyzer crystals, where a perfect flat single crystal is cross-grooved to form an array of several (typically 10^4) individual cubes, which are then arranged on a spherical surface (Baron *et al.*, 2001; Sinn *et al.*, 2001; Masciovecchio *et al.*, 1996*a*,*b*). In this way the contribution to the energy resolution caused by strain in the crystal, given by (1), is eliminated since the individual cubes behave as perfect crystals. However, now the finite cube size causes a contribution of

$$\Delta E/E = (c/R)\cot\theta_{\rm B}, \qquad (2)$$

where c is the length of the cube edge.

The cube-size contribution has this far been considered to be inevitable. The only ways of minimizing the effect have been to reduce the cube size c, to increase the Rowland circle diameter R and to increase the Bragg angle to as close to 90° as possible, *i.e.* to the backscattering geometry (Graeff & Materlik, 1982). Reducing the cube size faces mechanical limitations, and a part of the crystal is inevitably lost because of sawing and etching. Thus the smaller the cube size, the lower the efficiency of the analyzer. Increasing the Rowland circle diameter reduces the solid angle over which the photons are collected, the observed intensity decreasing as $1/R^2$.

The purpose of this article is to present a method in which the cube-size error is eliminated by using a two-dimensional position-sensitive pixel detector (PSD) and performing a dispersion-compensation correction to the data recorded by individual pixels. As an example, the method was applied in an experiment with an incident photon energy of 9.9 keV, a diced Si(555) crystal in a 1 m Rowland geometry (Verbeni *et al.*, 2005) and a Medipix2 detector (Llopart *et al.*, 2002). The 190 meV cube-size contribution to the resolution function was eliminated and a final resolution of 23 meV was achieved.

The article is arranged as follows. §2 presents results of a ray-tracing analysis and predictions of the performance of a diced analyzer crystal. §3 describes the corresponding experiment utilizing a diced analyzer crystal operating in a

near-backscattering geometry. The results are then discussed in §4, and conclusions presented in §5.

2. Ray-tracing results

A ray-tracing simulation was performed to study the performance of diced analyzer crystals. The simulation assumes the surface of the analyzer to be a mirror that reflects with 100% efficiency. No corrections for dynamical diffraction or strain/stress in the crystal are taken into account. The surface of the analyzer is treated numerically, so it can assume any shape. For simulation purposes, both the source and the detector can be displaced arbitrarily to study the effects of misalignment with respect to the Rowland circle configuration, and to observe how the focus and energy resolution depend on the geometry. The detector is a planar surface which records the position and the energy of the X-rays reflected by the analyzer. The point source is an isotropic emitter of polychromatic radiation, and the analyzer picks up the X-rays with energies that fall into its bandwidth determined by the various geometrical contributions.

For the present simulation, we assume a perfect spherically arranged grid of flat single crystals of dimensions 0.7 mm × 0.7 mm. Each dice is divided into a grid of 20 × 20 points. The analyzer was assumed to be a cross-grooved Si(555) wafer in the Johann geometry on a Rowland circle of diameter R = 1000 mm. The analyzer crystal diameter was taken to be 100 mm.

Fig. 1 depicts the results of the simulation, *i.e.* the focus and the energy distribution of the diced analyzer crystal when the mean Bragg angle is 88.5°. The result is a square focus of dimensions comparable with the size of an individual cube magnified by a factor of two. The image of the cube is magnified because an individual cube does not focus the X-rays but rather disperses them. Only a picture of a single cube is seen, since the images of all cubes are superimposed to a very good approximation, only hindered by the Johann error, which is minimal in this case. The colours in the figure correspond to the energy of the rays reflected by the analyzer. The most important result of this study is evident from Fig. 1 and can be described as follows. Each single cube is a flat crystal along which the Bragg angles of the incident rays vary. This variation corresponds to the cube-size effect of equation (2), and if the analyzed radiation is detected with a position-insensitive detector (PISD) the effect contributes directly to the resolution function. However, it is important to notice that if both the source and the detector lie on the Rowland circle then the radiation reflected with a specific Bragg angle by the cube surface is observed in a specific position in space in the focus. That is, there is a correspondence of the position and energy for the collected rays. The relationship follows directly from Bragg's law, and is $r/R = \sin 2\theta_B$, where r is the distance between the sample and the pixel that detects the photon. When $c \ll r$, the correspondence is linear within the focus to a good approximation, with a slope of

$$\mathrm{d}E/\mathrm{d}r = (E/2R)\cot\theta_B. \qquad (3)$$

At the utilized Bragg angle of 88.5°, the slope is predicted to be 130 meV mm^{-1}.

3. Experimental set-up and results

The experiment was performed at beamline ID16 of the European Synchrotron Radiation Facility (ESRF) utilizing a spectrometer based on a 1 m-diameter Rowland circle. The analyzer was a cross-grooved Si(555) crystal with a diameter of 100 mm and a cube size of 0.7 mm × 0.7 mm × 2.0 mm (Verbeni *et al.*, 2005).

Radiation from an undulator source was monochromated by a Si(111) double-crystal monochromator to a bandwidth of approximately 1.4 eV at 9.9 keV and further by a Si(555) backscattering channel-cut monochromator utilized at the same Bragg angle as the analyzer, namely 88.5°. The energy bandwidth of the monochromated X-rays was measured to be 15 meV, as expected from the Si(555) Darwin width value. Typical energy scans in a 500 meV range were performed by changing the Si(111) pre-monochromator and the channel-cut Bragg angles simultaneously. The radiation was focused after the second monochromator by a toroidal Rh-coated mirror. The intensity of the radiation at the sample was 10^{11} photons

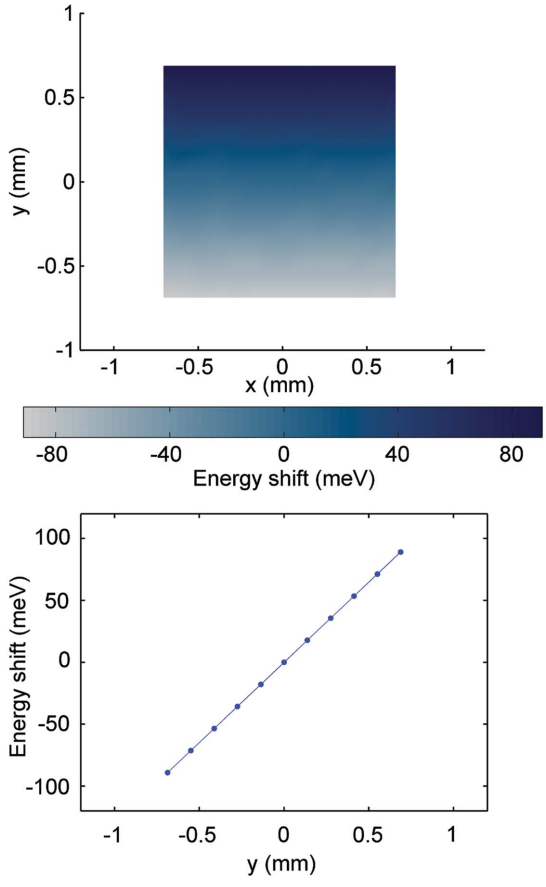

Figure 1
Upper panel: theoretical focus from the ray-tracing simulation. The intensity is predicted to be constant all over the focal area, and the pixel colour corresponds to the energy of the X-rays arriving at that pixel. Lower panel: relation between the pixel position and the energy shift from the nominal mean energy as predicted by the ray-tracing simulation.

s^{-1} (with an average synchrotron ring current of 100 mA) in a spot size of 150 µm × 40 µm (H × V). The sample was a Kapton foil of thickness 75 µm. Elastically scattered photons were observed with a momentum transfer of $q = 2.6$ Å^{-1}.

The X-rays collected by the analyzer were detected using a Medipix2 photon-counting pixel detector (Llopart *et al.*, 2002). The thickness of the silicon sensor was 300 µm. The sensitive area of the detector was 14 mm × 14 mm, consisting of 256 × 256 pixels, each pixel being a 55 µm × 55 µm square. Each pixel can count up to 8001 events per exposure at a maximum count rate of 1 MHz. The dark count rate was observed to be less than 10^{-5} counts s^{-1} $pixel^{-1}$. In the present experiment this noise level corresponded to about 0.005 counts s^{-1} over the focal area. The main reason for the noise is believed to be cosmic radiation, and further work will be carried out to minimize it using different ways of signal discrimination. The detector was positioned on the Rowland circle at a distance of 52 mm from the sample. The aluminium frame of the detector chip was 30 mm wide and the rest of the space was reserved for the sample environment. The experimental geometry is presented schematically in Fig. 2.

The experimentally observed focus was indeed found to be a square with dimensions of a single analyzer-crystal cube magnified by a factor of two, as expected. This result differs from that of Blasdell & Macrander (1995), where a round focus was observed. The experimental focus is shown in Fig. 3, and its projections along the sides of the square in Fig. 4. It should be stressed that to observe the square focus both the source and the detector have to lie on the Rowland circle. This requirement is very important if one wishes to perform the dispersion-compensation correction for the data utilizing the method that will be described below.

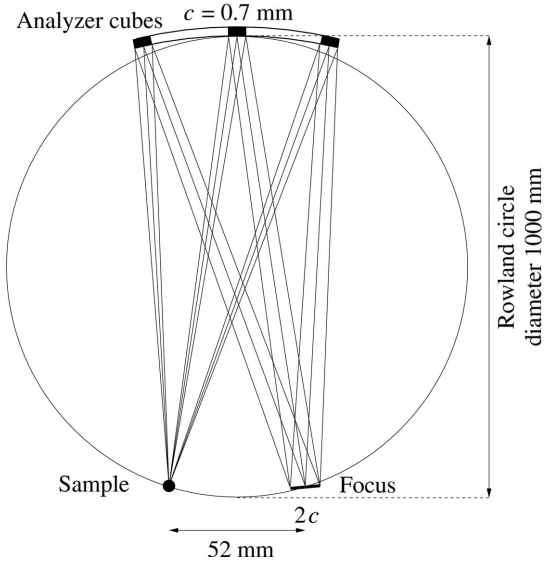

Figure 2
Scheme of the geometry used in the experiment. The spectrometer is based on a Rowland circle with a diameter of 1000 mm in the backscattering geometry. The analyzer consists of $\sim 10^4$ individual cubes with an edge length of c, resulting in a square focus with an edge length of $2c$. The operation of three selected cubes is shown.

The energy scans were performed by tuning the incident-photon energy (E) around the elastic line (E_0) in constant steps and recording the corresponding image on the PSD. The resulting series of images is shown in Fig. 5. Since the energy bandwidth of incident radiation was smaller than the cube-size contribution, it was observed that only a part of the focal spot was illuminated at a given incident-photon energy. It can be

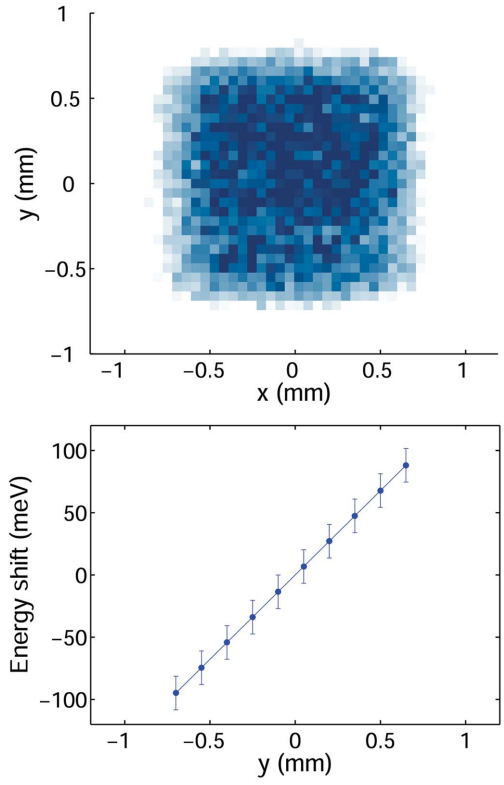

Figure 3
Upper panel: experimentally observed focus of the diced analyzer crystal. Lower panel: relation between the pixel position and the corresponding energy shift from the nominal mean energy as observed from the experimental data. The error bars represent the width of the resolution function of an individual pixel (27 meV), to which the contribution of the spectrometer was determined to be 23 meV.

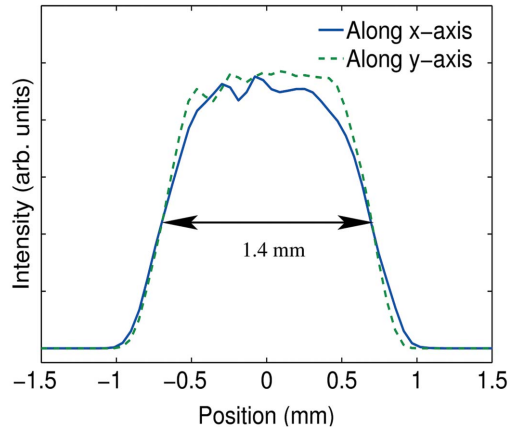

Figure 4
Projection of the focal image of Fig. 3 on axes parallel to the edges of the focal square. The full width at half-maximum of the focal image is 1.4 mm, consistent with a cube size of 0.7 mm magnified by a factor of two.

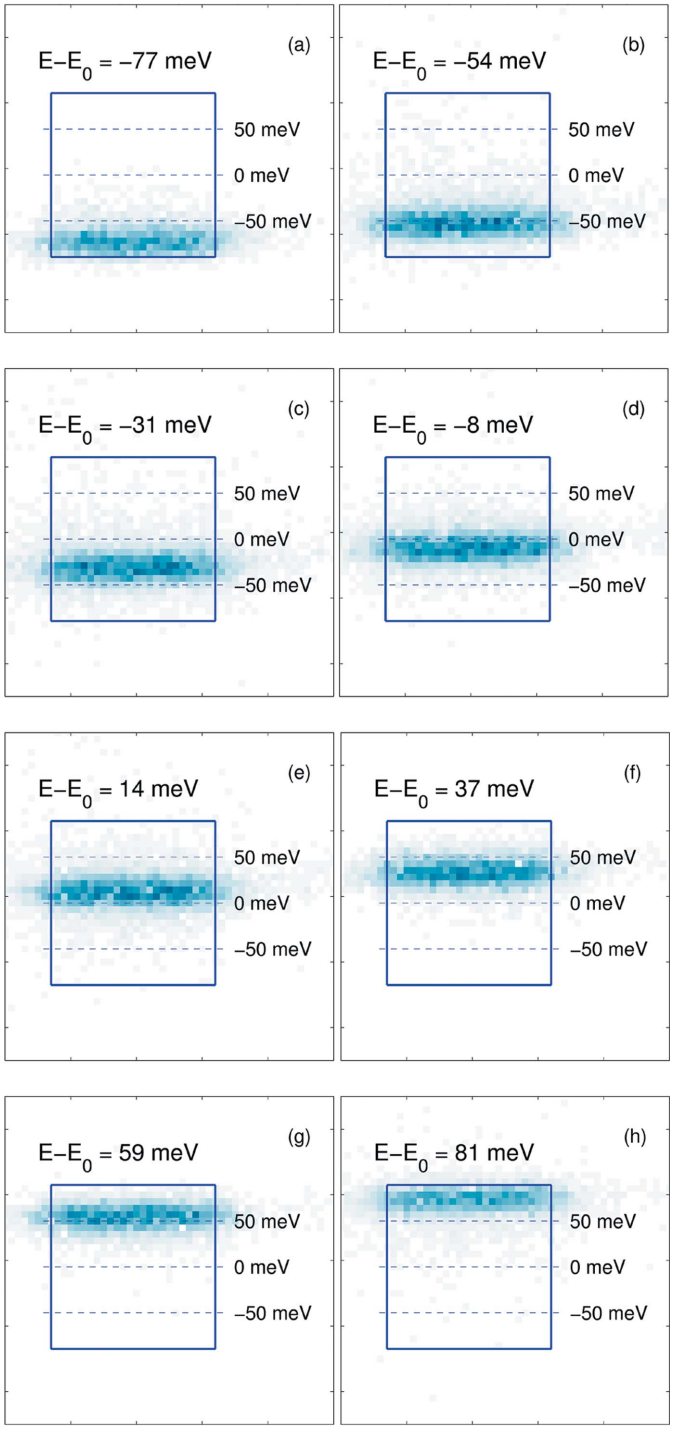

Figure 5
Series of images recorded by the PSD when the incident-photon energy E is tuned across the elastic line, which is centered at E_0. One can observe how only a part of the square focus of Fig. 3 is illuminated at a given incident energy, reflecting the fact that there is a well resolved correspondence between the position of a pixel and the X-ray energy detected by it. The bandwidth of the incident radiation was 15 meV. The ultimately achievable resolution after the dispersion-compensation correction corresponds to the finite width of the line that sweeps across the focus. In this case, one pixel has a bandwidth of 7 meV and the width of the line is about 4 pixels. The square is a guide for the eye depicting the focal dimensions of 1.4 mm × 1.4 mm.

Table 1
Contributions to the final resolution function of the present experiment.

When the finite incident bandwidth is deconvoluted from the measured resolution function, the resolution of the spectrometer itself is found to be 23 meV with an incident photon energy of 9.9 keV.

Contribution	ΔE (meV)
Analyzer Darwin width	15
Source size	10
Pixel size	7
Johann aberration	<1
Spectrometer	23
Incident bandwidth	15
Total	27

clearly seen how a specific part of the focus has a relationship with the corresponding energy. In fact, in accordance with the ray-tracing results, the relationship was found to be linear with a slope of 130 meV mm^{-1} at this Bragg angle.

The data recorded by the PSD can now be analyzed as follows. Taking the data of only those pixels that have a common y-coordinate in Fig. 3 is equivalent to analyzing only the intensity diffracted by a small part of an individual cube. Therefore, using a PSD with a pixel size $p \ll c$, the cube-size contribution of equation (2) in the resolution function is replaced by a pixel-size contribution,

$$\Delta E/E = (p/2R)\cot\theta_{\rm B}', \tag{4}$$

where $\theta_{\rm B}'$ is the Bragg angle of the X-ray diffracted by the cube surface and detected by a specific pixel. This angle may be different for each pixel, but unless the Bragg angle is very close to 90° one can assume that $\cot\theta_{\rm B}' \simeq \cot\theta_{\rm B}$. In this way the factor c/R in (2) is replaced by the factor $p/2R$. In the case of the present experiment, the pixel-size contribution was 7 meV, while the cube-size contribution would have been 190 meV.

Naturally, other contributions to the resolution function will become dominant after the above-described dispersion-compensation correction has been made. In the case of the present experiment the dominant contribution was the Darwin width of the Si(555) reflection (15 meV), determining both the incident bandwidth and the reflected bandwidth. Fig. 6 presents the resolution function of pixels lying on a few selected positions on the y-axis of the focus. In addition, Fig. 6 presents the resolution function when all pixels are simply summed together, *i.e.* if a PISD had been used to collect all the photons. It can be seen that when considering the data from single pixels (or lines of pixels) the resolution can be remarkably enhanced. The remaining resolution function in this case has a full width at half-maximum (FWHM) of 27 meV, consisting of the contributions that are reported in Table 1. When the finite incident bandwidth is not taken into account, the resolution of this 1 m Rowland spectrometer was observed to be 23 meV at 9.9 keV, *i.e.* the resolving power is 4.3×10^5. It should be noted that while the Johann aberration causes a maximum energy shift of 8 meV, its FWHM is less than 1 meV. The finite source size s contributes to the resolution function in the accustomed way, *i.e.* $\Delta E/E$ =

$(s/R)\cot\theta_B$, and will start to play a non-negligible role when the spectrometer Bragg angle is not close to 90°.

The improvement in the resolving power is demonstrated in Fig. 7, where a phonon spectrum of single-crystalline Be is shown as measured utilizing the 1 m Rowland circle spectrometer. The scattering vector was along the [001] direction, the momentum transfer being $q = 2.6$ Å^{-1}. Two acoustic phonon peaks together with a quasi-elastic line at zero energy transfer are seen. It is evident how the dispersion-compensation method conserves the total intensity and increases the resolving power dramatically.

4. Discussion

In non-resonant scattering experiments it is possible to choose the Bragg angle almost arbitrarily if the spectrometer is kept fixed and the energy of the incident photons is tuned instead. This technique permits the use of extreme backscattering (typically $\theta_B \simeq 89.98°$), where the cube-size contribution in (2) is diminished owing to the factor of $\cot\theta_B$. However, for very high resolution experiments, where resolution is in the meV range, one has at the same time to choose the Rowland circle diameter to be very large, *e.g.* 6.5 m at ESRF ID16 (Masciovecchio *et al.*, 1996*a*,*b*), in order to further reduce the cube-size contribution. Owing to these constraints there is basically no flexibility in the design of very high resolution spectrometers. We propose to use the introduced dispersion-compensation method to reduce these constraints. For example, this method may allow for a new design of high-resolution non-resonant inelastic X-ray scattering spectrometers based on much shorter Rowland circle diameters than the existing ones, thus reducing both the size and the cost of the spectrometers. Simultaneously the efficiency of the spectrometers can be enhanced since the increased solid angle will lead to an increase in the observed intensity.

The orientation of a diced analyzer crystal deserves a note even when the dispersion-compensation method is not used and a PISD is applied to detect the radiation. In those cases, where the cube-size contribution is the dominant factor in the resolution function, it is possible to modify the shape of the resolution function by simply choosing the orientation of the analyzer crystal. If the grooves are at an angle of 45° with respect to the plane of diffraction, the cube-size contribution becomes a triangular function with a FWHM of $(c/\sqrt{2}R)\cot\theta_B$. This might be the desired shape for a resolution function in cases where a small FWHM is needed. If the grooves are parallel to the plane of diffraction, the corresponding cube-size contribution is a boxcar function with a width of $(c/R)\cot\theta_B$ (see Fig. 8). This would be the desired shape when it is necessary to minimize the tails of the resolution function, *e.g.* for observation of weak excitations close to the elastic line.

If the dispersion-compensation method is utilized, the finite cube size does not play a role in the resolution function. It is possible, for instance, to choose a larger cube size to obtain a spectrum with a larger energy range at once. For example, a

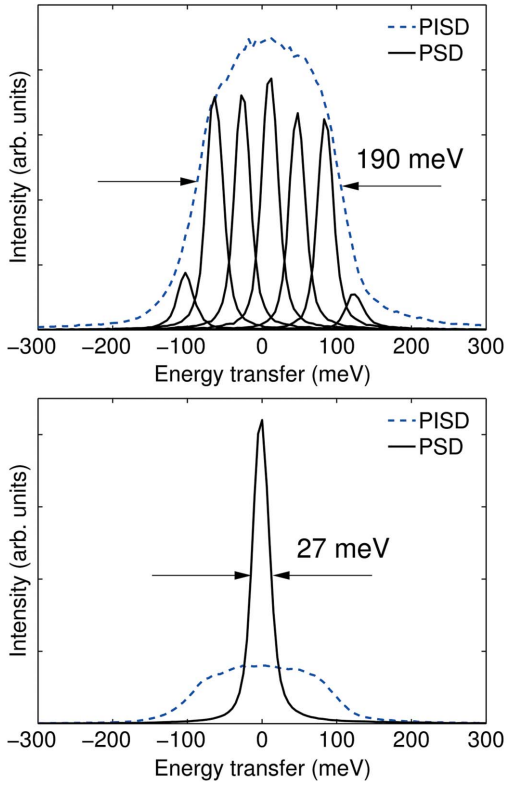

Figure 6
Results of data analyzed utilizing the PSD. The dashed line represents the resolution function when all the pixels are summed, *i.e.* it corresponds to data recorded with a PISD. The solid lines represent the resolution function when the linear position/energy-dependence is applied, and the images from the PSD are analyzed by summing over the pixels in the non-dispersive (horizontal) axis. The upper panel shows the resolution function for a series of lines of pixels, and the lower panel the final resolution function when the position–energy relationship has been utilized and the signals of all pixels are summed together. It can be clearly seen how resolution is increased without any loss of intensity.

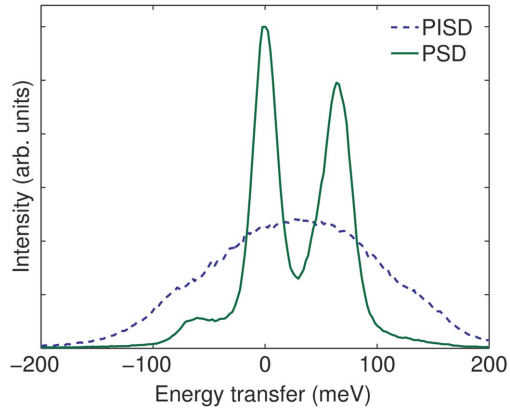

Figure 7
Acoustic phonons and elastic line in single-crystalline Be measured with and without the dispersion-compensation method, the total resolutions being 27 meV and 190 meV, respectively. The application of the described dispersion-compensation correction allows the quasi-elastic line to be resolved from the phonon peaks, which are smeared if the radiation is detected with a PISD. Note how the total intensity is conserved, the areas under both curves being equal, but the resolving power changes markedly.

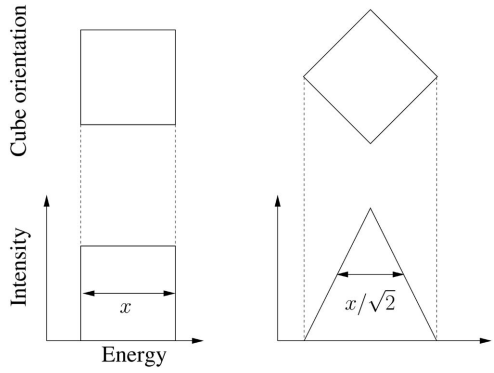

Figure 8
The orientation of the cubes *versus* the cube-size contribution to the resolution function. The cube-size contribution has a width of $x = (c/R)\cot\theta_B$ if the cubes are oriented so that their edges are along the diffraction plane, but the width is reduced to $x/\sqrt{2}$ if the edges are oriented at an angle of 45° with respect to the diffraction plane.

cube size of 5 mm would result in a 1.3 eV energy range in the focus at a Bragg angle of 88.5°.

Inelastic X-ray scattering spectrometers utilizing dispersion-compensation methods (Berthold *et al.*, 1992; Suortti *et al.*, 2001) and PSDs (Bortel *et al.*, 2000; Tohji & Udagawa, 1987) have also been constructed earlier. Most interesting is perhaps the spectrometer of Hämäläinen *et al.* (1995), where a cylindrically bent crystal was used instead of a spherical diced analyzer, and the utilized non-dispersive geometry corresponds to the use of the cube surface as an energy-analyzing element in the present experiment. The most important advantage of diced analyzer crystals over cylindrically bent ones is that all problems related to bending, for example the bending error of equation (1) and anticlastic bending (Krisch *et al.*, 1991), are avoided, thus allowing for a much higher energy resolution. It should be noted that in the previous designs of spectrometers that were based on the use of PSDs the non-linearity of the utilized detectors and the low signal-to-noise ratio reduced the possibilities to perform high-accuracy experiments. It has been mainly the development of low-noise high-resolution photon-counting PSDs like the Medipix2 that makes this type of inelastic X-ray scattering experiments feasible today.

5. Conclusions

Results of a ray-tracing simulation and of an experiment performed with a diced-crystal spectrometer operating in a 1 m Rowland circle geometry prove that it is possible to improve the resolution function of diced analyzer crystals by utilizing a position-sensitive detector and performing a dispersion-compensation correction to the data recorded by individual pixels. This corresponds to replacing the so-called cube-size contribution in the resolution function by a pixel-size contribution which is governed by the type of detector used. The suggested method should open up new possibilities for enhancing the performance of high-resolution X-ray spectrometers in resonant inelastic X-ray scattering, non-resonant inelastic X-ray scattering and in emission spectroscopy. As an example, the cube-size contribution of 190 meV was removed and a 23 meV resolution at a photon energy of 9.9 keV was achieved with a spectrometer based on a 1 m Rowland circle and a diced analyzer crystal in a near-back-scattering geometry. The utilization of the dispersion-compensation method preserves all counted photons so that the improvement in resolution is not accompanied by any loss of intensity.

References

Baron, A. Q. R., Tanaka, Y., Miwa, D., Ishikawa, D., Mochizuki, T., Kimura, H., Yamamoto, F. & Ishikawa, T. (2001). *SPring-8 Information 6*, pp. 99–102. SPring-8, Hyogo, Japan.
Berthold, A., Mourikis, S., Schmitz, J. R., Schülke, W. & Schulte-Schrepping, H. (1992). *Nucl. Instrum. Methods A*, **317**, 373–382.
Blasdell, R. C. & Macrander, A. T. (1995). *Rev. Sci. Instrum.* **66**, 2075–2077.
Bortel, G., Alp, E. E., Sturhahn, W. & Toellner, T. S. (2000). *J. Synchrotron Rad.* **7**, 333–339.
Graeff, W. & Materlik, G. (1982). *Nucl. Instrum. Methods*, **195**, 97–103.
Hämäläinen, K., Krisch, M., Kao, C.-C., Caliebe, W. & Hastings, J. B. (1995). *Rev. Sci. Instrum.* **66**, 1525–1527.
Johann, H. H. (1931). *Z. Phys.* **69**, 185–206.
Krisch, M., Freund, A., Marot, G. & Zhang, L. (1991). *Nucl. Instrum. Methods A*, **305**, 208–213.
Llopart, X., Campbell, M., Dinapoli, R., San Segundo, D. & Pernigotti, E. (2002). *IEEE Trans. Nucl. Sci.* **49**, 2279–2283.
Masciovecchio, C., Bergmann, U., Krisch, M., Ruocco, G., Sette, F. & Verbeni, R. (1996*a*). *Nucl. Instrum. Methods B*, **111**, 181–186.
Masciovecchio, C., Bergmann, U., Krisch, M., Ruocco, G., Sette, F. & Verbeni, R. (1996*b*). *Nucl. Instrum. Methods B*, **117**, 339–340.
Sinn, H., Alp, E. E., Alatas, A., Barraza, J., Bortel, G., Burkel, E., Shu, D., Sturhahn, W., Sutter, J. P., Toellner, T. S. & Zhao, J. (2001). *Nucl. Instrum. Methods A*, **468–468**, 1545–1548.
Suortti, P., Buslaps, T., DiMichiel, M., Honkimäki, V., Lienert, U., McCarthy, J. E., Merino, J. M. & Shukla, A. (2001). *Nucl. Instrum. Methods A*, **467–468**, 1541–1544.
Suortti, P. & Freund, A. K. (1989). *Rev. Sci. Instrum.* **60**, 2579–2585.
Tohji, K. & Udagawa, Y. (1987). *Phys. Rev. B*, **36**, 9410–9412.
Verbeni, R., Kocsis, M., Huotari, S., Krisch, M., Monaco, G. & Vanko, Gy. (2005). *J. Phys. Chem. Solids.* Accepted.